FLEXURAL/TENSILE-STRENGTH RATIO IN ENGINEERED CEMENTITIOUS COMPOSITES

By Mohamed Maalej[1] and Victor C. Li,[2] Members, ASCE

ABSTRACT: In this paper the flexural behavior of a strain-hardening engineered cementitious composite (ECC) is studied and compared with that observed in a regular fiber-reinforced cementitious composite (FRC). Unlike concrete or regular FRC, ECC materials are characterized by their ability to sustain higher levels of loading after first cracking while undergoing additional straining. This strain-hardening behavior gives ECCs a significant advantage under flexural loading. In quasi-brittle material such as regular FRC, the ratio of flexural strength (the modulus of rupture) to tensile strength is known to vary between 1 and 3, depending on the details of the reinforcement and the geometry of the specimen. In this paper, the strain-hardening behavior observed in an ECC led to a high flexural-strength–to–tensile-strength ratio. In a third-point bending test, the flexural strength of an ECC was measured to be five times its tensile (first-cracking) strength. This result was also predicted by a simple theoretical model. The model can be used for the purpose of optimizing the flexural strength of ECCs.

INTRODUCTION

Three types of tensile failure modes have been observed in cementitious materials (see Fig. 1 for a schematic illustration): brittle, quasi-brittle, and ductile failure. Brittle failure can be observed in hardened cement paste material. It is characterized by a linear stress-strain curve (curve A) followed by a sudden drop in stress at first cracking with an ultimate tensile strain in the order of 0.01%. Quasi-brittle failure can be observed in concrete and most fiber-reinforced cements and concretes. It is characterized by a linear stress-strain curve (curve B) followed by a softening tail (tension-softening curve), after first cracking, due to the bridging action of aggregates, cement ligaments, and/or fibers. The ultimate tensile strain of quasi-brittle materials is of the same order of magnitude as that for brittle materials, although the material toughness is enhanced by inelastic energy absorption in the post-peak regime. For both brittle and quasi-brittle materials, the first cracking strength corresponds to the tensile strength of the material. Ductile failure can be observed in continuous aligned fiber-reinforced cement materials (Aveston et al. 1974; Krenchel and Stang 1988). Ductile materials are characterized by their ability to sustain higher levels of loading after first cracking while undergoing large deformation (curve C). Recently ductile failure has also been observed in short-fiber cementitious composites of low-fiber-volume fractions (Li 1993; Li and Hashida 1992) (e.g., 2% for polyethylene-fiber composites). These composites have been designed according to micromechanical models that are constructed on the basis of micromechanics of defect growth in a brittle matrix composite whereby crack bridging is provided by fibers to achieve steady state cracking (Li and Leung 1992;

[1]Res. Fellow, Advanced Civ. Engrg. Mater. Res. Lab., Dept. of Civ. and Envir. Engrg., Univ. of Michigan, 2326 G.G. Brown Bldg., Ann Arbor, MI 48109-2125.

[2]Prof., Advanced Civ. Engrg. Mater. Res. Lab., Dept. of Civ. and Envir. Engrg., Univ. of Michigan, Ann Arbor, MI.

Note. Discussion open until April 1, 1995. To extend the closing date one month, a written request must be filed with the ASCE Manager of Journals. The manuscript for this paper was submitted for review and possible publication on January 24, 1994. This paper is part of the ***Journal of Materials in Civil Engineering***, Vol. 6, No. 4, November, 1994. ©ASCE, ISSN 0899-1561/94/0004-0513/$2.00 + $.25 per page. Paper No. 7737.

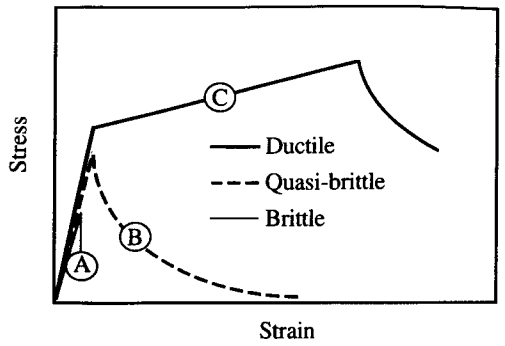

FIG. 1. Three Types of Failure Modes Observed in Cementitious Materials

Marshall and Cox 1988). These composites are referred to as strain-hardening engineered cementitious composites (ECC). The ductile failure mode gives ECC materials a large strain capacity when compared with the matrix alone (e.g., 0.5% for steel-fiber composites and 5.4% for polyethylene-fiber composites).

The flexural strength of cement-based materials is known to depend on their tensile failure mode. Hillerborg et al. (1976) and Zhu (1990) showed that the flexural strength of concrete depends on a parameter called the brittleness ratio, which is a function of material properties and specimen geometry. In particular, they showed that the flexural strength of concrete depends on the material fracture resistance that can be described by a stress crack-opening law called the tension-softening relation (σ-δ). Maalej and Li (1994) studied the flexural strength of quasi-brittle fiber cementitious composites. They showed that the ratio of flexural strength to tensile strength varies as a function of the brittleness ratio B, defined in their study as $T_b d/E_c w_c$, where T_b and E_c are the postcracking strength and the elastic modulus of the composite, w_c is the crack opening at which the bridging stress vanishes, and d is the depth of the specimen. The ratio of flexural strength to tensile strength decreases with increasing brittleness ratio. In the limiting case when B is infinite, corresponding to linear elastic brittle behavior of the material, the flexural strength is equal to the tensile strength as predicted by the linear elastic brittle theory. In the other limiting case, $B \rightarrow 0$, the ratio of flexural strength to tensile strength is equal to 3, as predicted by elastic–perfectly plastic theory.

In an unnotched beam specimen made of a regular (quasi-brittle) fiber-reinforced concrete (FRC), first cracking is accompanied by the development of a localized fracture process zone. In this process zone, the bridging fibers can partially transfer the stress across the crack; however, the magnitude of the transferred stress decreases as the crack enlarges. Therefore, no additional cracks will form beyond this first crack. During this process, energy due to fiber frictional pull-out is being consumed. Because of this energy absorption, the flexural strength of regular FRC is higher than its tensile strength (Maalej and Li 1994; Ward and Li 1990). In contrast, in an unnotched beam specimen made of an ECC material, first cracking is accompanied by a strain concentration at the mouth of the crack. Because of the stress transfer capability of the reinforcing fibers in a strain-hardening material, stress redistribution will occur so that localized fracture will be delayed. Consequently, an expanded zone of matrix cracking (parallel to

the first crack near the tensile face of the beam) must develop prior to localized fracture. Such an extensive volumetric cracking process must involve considerable energy absorption that is expected to give rise to a high ratio of flexural strength (the modulus of rupture [MOR]) to tensile (first-cracking) strength. An experimental program consisting of third-point bending tests performed on strain-hardening ECC as well as quasi-brittle FRC is designed to confirm this point. A theoretical model for predicting the flexural strength in strain-hardening ECC is also presented. The model results are compared to the experimental data obtained from the third-point bending tests of the ECC material.

FLEXURAL BEHAVIOR OF STRAIN HARDENING ECC

Regular FRC materials have an advantage under flexural loading due to their quasi-brittle behavior. This can be seen in their flexural strength, which is greater than their uniaxial tensile strengths. However, ECC materials have an additional advantage under flexural loading due to their strain-hardening behavior after first cracking. Because of the strain-hardening behavior of ECC materials, an expanded zone of multiple cracks develops in the flexural beam leading to a high flexural-strength–to–tensile-strength ratio. As will be shown later, this ratio is greater than 3, which is the upper limit of the flexural-strength–to–tensile-strength ratio for quasi-brittle materials. The following experimental program was designed to confirm this phenomenon with laboratory experiments.

Experimental Program

The materials used in this study were fiber-reinforced cement paste and fiber-reinforced mortar. The dimensions and mechanical properties of the fibers used for reinforcement are given in Table 1. The constituent materials of the matrices and their mix proportions are given in Table 2. Type 1 portland cement, silica fume, and superplasticizer were used to form the cement paste with a water-to-cement ratio of 0.30. The mortar had the same constituents as the cement paste, in addition to the silica sand (maximum grain size of 0.6 mm). Steel fibers were used to reinforce the mortar matrix

TABLE 1. Dimensions and Mechanical Properties of Fibers

Fiber (1)	Fiber diameter (μm) (2)	Fiber length (mm) (3)	Elastic modulus (GPa) (4)	Fiber strength (MPa) (5)	Fiber density (g/cm³) (6)
Steel	150	6	200	2500	7.8
Polyethylene	38	12.7	120	2700	0.98

TABLE 2. Matrix Mix Proportions (by Weight)

Matrix (1)	Cement (2)	Sand (3)	Silica fume (4)	Super-plasticizer (5)	Water[a] (6)
Mortar	1.00	0.75	0.10	0.02	0.30
Cement paste	1.00	0	0.10	0.01	0.30

[a]Water-to-cement ratio.

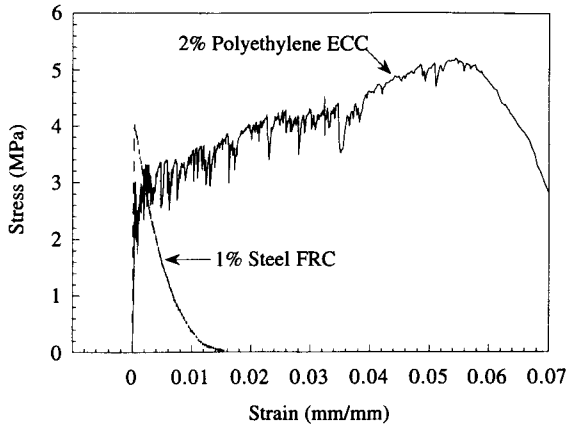

FIG. 2. Comparison between Uniaxial Tensile Stress-Strain Response of Quasi-brittle Material and that of Strain-Hardening Material

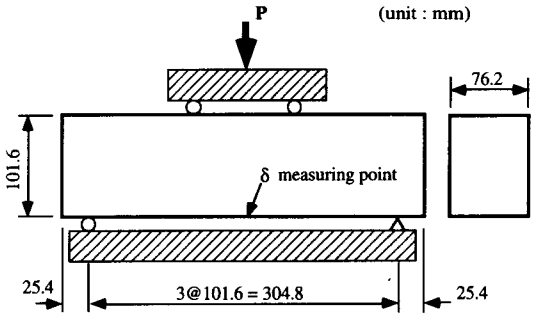

FIG. 3. Geometry of Bending Specimens

with a fiber-volume fraction of 1%, and polyethylene fibers were used to reinforce the cement paste matrix with a fiber-volume fraction of 2%. Examination of the strain-hardening conditions as outlined by Li and Leung (1992) indicated that the polyethylene-fiber composite and the steel-fiber composite can exhibit strain-hardening behavior if the fiber-volume fraction is greater than 0.7% and 8.5%, respectively. This means that the polyethylene-fiber composite is expected to exhibit strain-hardening behavior, and the steel-fiber composite is expected to exhibit quasi-brittle behavior. Fig. 2, which shows a comparison between the uniaxial tensile stress-strain curves of the two materials, indicates that this is indeed the case. The curve corresponding to the polyethylene-fiber composite shows a clear strain-hardening behavior with a tensile strain at peak stress approximately equal to 5.4% (about 500 times the strain capacity of the unreinforced matrix) (Li 1993). For this composite, real-time observation showed that multiple cracking occurred with many subparallel cracks across the specimen during strain hardening. Beyond peak stress, localized crack extension occurred, accompanied by fiber bridging. The second curve, corresponding to the steel-fiber composite, shows the behavior of a quasi-brittle material. After first cracking, the specimen failed by a decaying bridging stress (Li et al. 1994).

The flexural beam specimens were cast using Plexiglas molds. After casting, they were allowed to harden at room temperature for 1 day prior to demolding, then cured in water for 4 weeks before testing. A thin white coating of lime was applied on the specimens prior to testing to monitor the development of cracks better. The age at testing of all specimens was 29–30 days. The geometry and loading configuration of the flexural beam specimens are shown in Fig. 3. This experimental setup is recommended in ASTM C78-75, the standard test method of flexural strength of concrete (using a simple beam with third-point loading) ("Standard" 1983). One size of the beam is used in this experimental program. The total length, height, and width of the beam are 355.6 mm, 101.6 mm, and 76.2 mm, respectively. The midspan length, 101.6 mm, is one-third of the span length, 304.8 mm.

The flexural tests were conducted in a hydraulic servo-controlled testing machine. The specimens were loaded to complete failure with a constant cross head speed. The load, head displacement of the machine, and deflection of the beams at the middle point were recorded in each test (see Fig. 3).

Results

For the steel-fiber composite, the first crack started inside the midspan at the tensile face of the flexural beams, and propagated toward the compressive face. The first crack developed as a single large crack in the midspan during the test. For the polyethylene-fiber composite, the first crack started inside the midspan at the tensile face, and multiple cracks developed from the first-cracking point and spread to the outside of the midspan. The multiple cracks in the outside of the midspan were inclined cracks similar to shear cracks in steel reinforced-concrete (RC) beams. As the MOR is approached, one of the cracks inside the midspan started to open up after a large damage zone had been developed. The through-thickness damage zone can reach an areal dimension of 200 cm^2. Fig. 4 shows a typical cracking pattern that develops in the beam middle span around the peak load.

Therefore, while the beams with the steel-fiber reinforcement failed by developing a localized single crack, the beams with the polyethylene-fiber reinforcement failed by developing distributed multiple cracks. This behavior is somewhat analogous to the multiple cracking commonly observed in a steel RC beam. However, the present polyethylene ECC beam does not employ steel rebar. Stress transfer is fully carried by the randomly distributed fibers.

The flexural stress-deflection curves for three specimens of each material are shown in Fig. 5. For the steel-fiber composite, the flexural stress increases rapidly to the peak value, then starts to decay. The average beam deflection at peak stress is about 0.4 mm. For the polyethylene-fiber composite, however, the flexural stress increases at a slower rate. This increase is accompanied by the development of multiple fine cracks. The average beam deflection at peak stress is about 7.4 mm. The flexural strength (MOR) for three specimens of each material is shown in Table 3. The ultimate flexural stress is considered as the flexural strength of each material. The ratios of flexural strength to first-cracking strength in uniaxial tension are also shown in Table 3. As indicated, the ratio of flexural strength to first-cracking strength is equal to 2.1 for the steel-fiber composite. This ratio is indeed between 1 and 3 as expected for a quasi-brittle material. However, the ratio in the strain-hardening polyethylene fiber composite is 5.0. This large increase in the ratio of flexural strength to first-cracking strength must

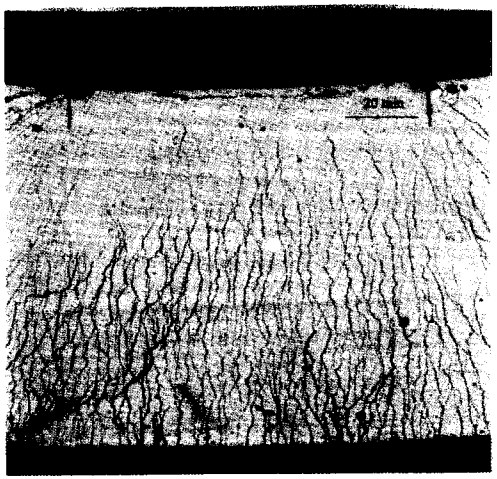

FIG. 4. Cracking Pattern in Beam Middle Span around Peak Load

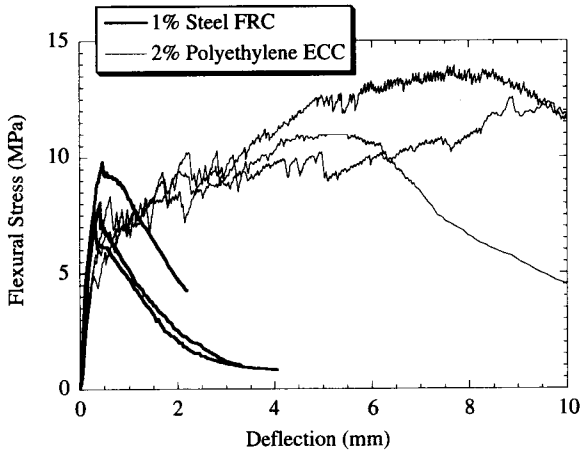

FIG. 5. Comparison between Flexural Stress-Deflection Curves of Quasi-brittle Material and that of Strain-Hardening Material

be related to the strain-hardening behavior of the polyethylene-fiber composite material.

THEORETICAL MODELING OF FLEXURAL STRENGTH OF STRAIN HARDENING ECC

Consider a rectangular beam with a width b and depth d, loaded in bending. The beam is made of an ECC material that, when loaded in uniaxial tension, exhibits a strain hardening behavior characterized by the stress-strain curve shown in Fig. 6. In uniaxial compression, the behavior of the ECC material is characterized by the stress-strain curve shown in Fig. 7. To simplify the analysis, we assume that the stress-strain behavior of the ECC

TABLE 3. Comparison of MOR and First Crack Strength

Material (1)	Specimen number (2)	MOR (MPa) (3)	MOR-to-σ_{tc} ratio[a] (4)
1% Steel FRC	1	8.07	2.01
1% Steel FRC	2	7.72	1.92
1% Steel FRC	3	9.81	2.44
1% Steel FRC	Average	8.53	2.12
2% Polyethylene	1	10.97	4.40
ECC	2	12.57	5.03
ECC	3	13.94	5.58
ECC	Average	12.49	5.00

[a]The tensile first-cracking strength σ_{tc} is 4.02 MPa for the 1% steel FRC (Li et al. 1994), and 2.50 MPa for the 2% polyethylene ECC (Maalej 1994). These were obtained from direct uniaxial tensile tests.

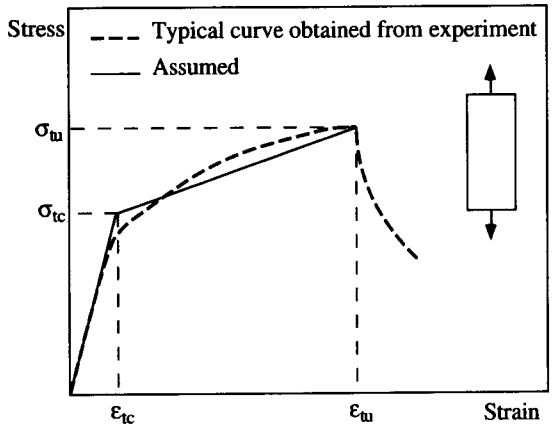

FIG. 6. Stress-Strain Behavior of ECC in Uniaxial Tension

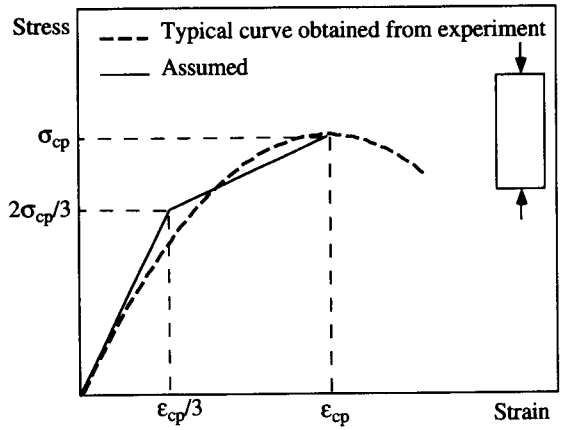

FIG. 7. Stress-Strain Behavior of ECC in Uniaxial Compression

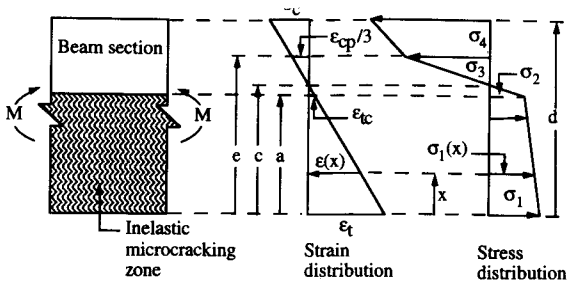

FIG. 8. Strain and Stress Distribution along Beam Depth

material in uniaxial tension and compression can be described by bilinear stress-strain curves as shown in solid line in Figs. 6 and 7, respectively. Fig. 8 shows the portion of the beam subjected to the highest bending moment M. The strain in the beam is assumed to vary linearly along its depth. In this case, the stress distribution along the beam depth is given by:

$$\sigma(x) = \sigma_1(x) = \sigma_{tc} + \frac{\sigma_{tu} - \sigma_{tc}}{\varepsilon_{tu} - \varepsilon_{tc}}[\varepsilon(x) - \varepsilon_{tc}] \qquad \text{for } 0 \le x \le a \qquad (1a)$$

$$\sigma(x) = \sigma_2(x) = \frac{\sigma_{tc}}{\varepsilon_{tc}}\varepsilon(x) \qquad \text{for } a \le x \le c \qquad (1b)$$

$$\sigma(x) = \sigma_3(x) = -2\frac{\sigma_{cp}}{\varepsilon_{cp}}\varepsilon(x) \qquad \text{for } c \le x \le e \qquad (1c)$$

$$\sigma(x) = \sigma_4(x) = -\frac{1}{2}\sigma_{cp}\left[1 + \frac{\varepsilon(x)}{\varepsilon_{cp}}\right] \qquad \text{for } e \le x \le d \qquad (1d)$$

where σ_{tc} = tensile first-cracking strength; ε_{tc} = tensile first-cracking strain; σ_{tu} = ultimate tensile strength; ε_{tu} = ultimate tensile strain; σ_{cp} = compressive strength; ε_{cp} = compressive strain at peak stress; ε_t = tensile strain at the extreme tension fiber; $\varepsilon(x)$ = strain at point $x = (x/a)(\varepsilon_{tc} - \varepsilon_t) + \varepsilon_t$ for $0 \le x \le c$ and $(x/a)(\varepsilon_t - \varepsilon_{tc}) - \varepsilon_t$ for $c \le x \le d$; x = distance from the extreme tension fiber to an arbitrary point along the depth of the beam; a = depth of inelastic microcracking zone; c = distance from the extreme tension fiber to the neutral axis = $a\varepsilon_t/(\varepsilon_t - \varepsilon_{tc})$; and e = distance from the extreme tension fiber to the point where the material changes stiffness in compression = $a(\varepsilon_{cp} - 3\varepsilon_t)/(3\varepsilon_t - 3\varepsilon_{tc})$.

The stress and strain distribution for the beam section and the distances x, a, c, and e are indicated in Fig. 8. We can now write the equilibrium equations for the beam section—namely, the sum of normal forces is equal to zero and the moment of the normal forces is equal to the external bending moment M.

$$\int_0^a b\sigma_1(x)\,dx + \int_a^c b\sigma_2(x)\,dx + \int_c^e b\sigma_3(x)\,dx + \int_e^d b\sigma_4(x)\,dx = 0 \qquad (2a)$$

$$\int_0^a b\sigma_1(x)x\,dx + \int_a^c b\sigma_2(x)x\,dx + \int_c^e b\sigma_3(x)x\,dx + \int_e^d b\sigma_4(x)x\,dx = M \qquad (2b)$$

The equilibrium equations are solved such that the external bending moment M and the tensile strain at the extreme tension fiber ε_t can be expressed as functions of the known material parameters and specimen geometric dimensions, and the size of the microcracking zone a. Eqs. (2a) and (2b) can be analytically solved for M and ε_t such that:

$$M = M(\sigma_{tc}, \varepsilon_{tc}, \sigma_{tu}, \varepsilon_{tu}, \sigma_{cp}, \varepsilon_{cp}, r, b, d) \qquad (3a)$$

$$\varepsilon_t = \varepsilon_t(\sigma_{tc}, \varepsilon_{tc}, \sigma_{tu}, \varepsilon_{tu}, \sigma_{cp}, \varepsilon_{cp}, r) \qquad (3b)$$

where $r = a/d$. The actual expressions for M and ε_t are given in Appendix I.

In this paper, we assume the beam fails when the applied moment is equal to the ultimate moment capacity of the beam. Furthermore, we assume that the beam fails by exhausting the strain capacity of the material either at the tensile face ($\varepsilon_t > \varepsilon_{tu}$) or at the compressive face ($\varepsilon_c > \varepsilon_{cp}$). In this case the ultimate moment capacity M_u is given by:

$$M_u = M(\sigma_{tc}, \varepsilon_{tc}, \sigma_{tu}, \varepsilon_{tu}, \sigma_{cp}, \varepsilon_{cp}, r_u, b, d) \qquad (4)$$

where $r_u = \min(r_t, r_c)$ such that:

$$\varepsilon_t(\sigma_{tc}, \varepsilon_{tc}, \sigma_{tu}, \varepsilon_{tu}, \sigma_{cp}, \varepsilon_{cp}, r_t) = \varepsilon_{tu} \qquad (5a)$$

$$\varepsilon_c(\sigma_{tc}, \varepsilon_{tc}, \sigma_{tu}, \varepsilon_{tu}, \sigma_{cp}, \varepsilon_{cp}, r_c) = \varepsilon_{cp} \qquad (5b)$$

and

$$\varepsilon_c = \varepsilon_c(\sigma_{tc}, \varepsilon_{tc}, \sigma_{tu}, \varepsilon_{tu}, \sigma_{cp}, \varepsilon_{cp}, r) = \frac{1 - r}{r}\varepsilon_t(\sigma_{tc}, \varepsilon_{tc}, \sigma_{tu}, \varepsilon_{tu}, \sigma_{cp}, \varepsilon_{cp}, r) - \frac{1}{r}\varepsilon_{tc} \qquad (6)$$

The flexural stress corresponding to M is given by:

$$\sigma_f = \frac{6M}{bd^2} = \sigma_f(\sigma_{tc}, \varepsilon_{tc}, \sigma_{tu}, \varepsilon_{tu}, \sigma_{cp}, \varepsilon_{cp}, r) \qquad (7)$$

and the modulus or rupture (MOR) corresponding to M_u is given by:

$$\text{MOR} = \sigma_f(\sigma_{tc}, \varepsilon_{tc}, \sigma_{tu}, \varepsilon_{tu}, \sigma_{cp}, \varepsilon_{cp}, r_u) \qquad (8)$$

The deformation of the beam associated with an applied moment M can be described by its curvature. Based on geometrical considerations, the beam curvature can be computed as the ratio of strain in the extreme tensile fiber to the distance from the extreme tensile fiber to the neutral axis (see Fig. 9):

$$\frac{1}{\rho} = \frac{\varepsilon_t}{c} \qquad (9)$$

For a constant curvature, the maximum deflection for a beam having a span L is given by:

$$u = \frac{L^2}{8\rho} \qquad (10)$$

The moment-curvature (or flexural stress-curvature) diagram of a beam can be computed by using (3a) and (9) [or (7) and (9)] and allowing r to

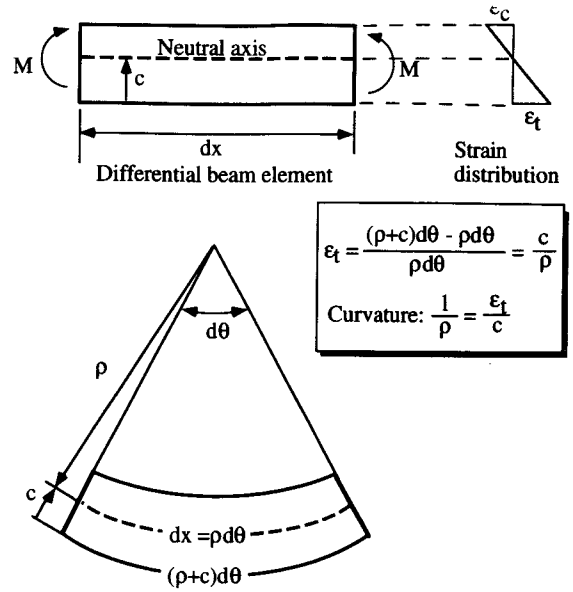

FIG. 9. Curvature of Differential Beam Element

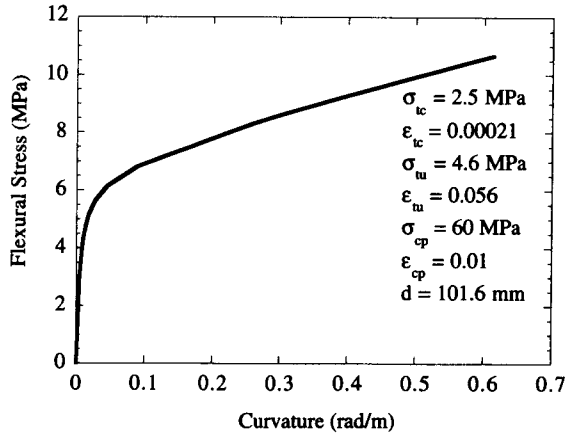

FIG. 10. Predicted Stress-Curvature Diagram for 2% Polyethylene ECC

vary between 0 and r_u. When r is small, the compressive stress distribution within the beam is linear. The solution for M and ε_t for this case is given in Appendix II. These equations should be used for all r values yielding $\varepsilon_c \leq \varepsilon_{cp}/3$ (see Fig. 7). When a selected r value yields $\varepsilon_c > \varepsilon_{cp}/3$, the equations for M and ε_t given Appendix I should be used instead for this r value, and other r values are less than or equal to r_u. Fig. 10 shows the predicted flexural stress-curvature diagram for a beam made of an ECC material. The depth of the specimen and the tensile and compressive properties of the ECC material used in the computation are also shown in Fig. 10. These

properties have been experimentally measured (Mishra 1993) for a 2% polyethylene ECC, which is the composite tested in flexure and discussed earlier. Interpretation of the computations that led to Fig. 10 indicates that first cracking occurs when the flexural stress in the beam is equal to 2.5 MPa. Then the microcracking zone (of size a) starts to move up from the extreme tensile fiber toward the extreme compressive fiber. At the same time, the position of the neutral axis is moving away from the centroid of the beam cross section toward the extreme compressive fiber. This is accompanied by a continuous decrease in the stiffness of the beam. Initially, the compressive stress distribution within the beam is linear. After a certain propagation of the microcracking zone, the compressive stress distribution becomes bilinear. The maximum moment is reached when the tensile strain in the extreme tensile fiber reaches the ultimate tensile strain of the ECC material. At that moment, the size of the microcracking zone (a) is about 90% of the beam depth. As shown in Fig. 4, this result is consistent with the experimentally observed microcracking zone size around the peak load.

In a third-point bending test of an ECC material, if we make the as-

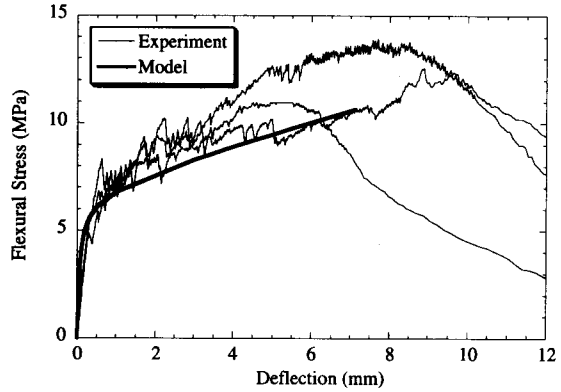

FIG. 11. Comparison between Predicted and Experimentally Measured Flexural Stress-Deflection Curves for 2% Polyethylene ECC

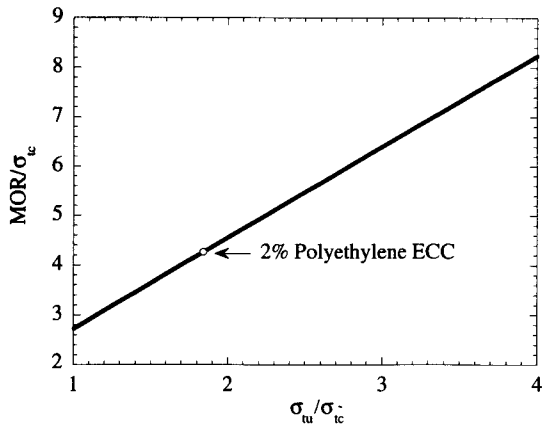

FIG. 12. Variation of MOR-to-σ_{tc} Ratio as Function of σ_{tu}/σ_{tc} Ratio

sumption that the curvature is approximately constant along the length of the beam and equal to the curvature in the middle span, we can predict the load-deflection curve of the beam. Fig. 11 shows the predicted and measured load deflection curves for the 2% polyethylene ECC. As indicated, there is a reasonable agreement between the predicted and the measured curves. This suggests that the theoretical model can be used to predict the load-deflection behavior of ECC materials.

Fig. 12 shows the variation of the ratio of flexural strength to tensile first-cracking strength (MOR-to-σ_{tc}) as a function of the ratio of ultimate tensile strength to tensile first-cracking strength (σ_{tu}/σ_{tc}) for the 2% polyethylene ECC (assuming that σ_{tc} and σ_{tu} can be varied without changing the other properties of the composite). As indicated, the MOR-to-σ_{tc} ratio increases linearly as a function of the σ_{tu}/σ_{tc} ratio. The MOR-to-σ_{tc} ratio varies between 2.7 and 8.3 as the σ_{tu}/σ_{tc} ratio varies betwen 1 and 4. In this case it is evident that when we increase σ_{tu} as σ_{tc} is held constant, the result would be an increase in the MOR-to-σ_{tc} ratio as well as in the MOR value. However, when σ_{tc} is decreased as σ_{tu} is held constant, the result would be an increase in the MOR-to-σ_{tc} ratio but a decrease in the MOR value.

Fig. 13 shows the variation of the MOR/σ_{tc} ratio as a function of the ultimate tensile strain (ε_{tu}) for the 2% polyethylene ECC (assuming that ε_{tu} can be varied without changing the other properties of the composite). This figure indicates that the MOR-to-σ_{tc} ratio increases as a function of ε_{tu}. The rate of increase is initially high, and as ε_{tu} becomes larger than 0.01, the rate of increase becomes very small. The model indicates that the initial high slope of the MOR/σ_{tc}-ε_{tu} curve is associated with a significant increase in the size of the microcracking zone as the ultimate tensile strain increases. When ε_{tu} becomes large, the size of the microcracking zone reaches about 90% of the beam depth and does not significantly change as ε_{tu} continues to increase. This suggests that the MOR of the 2% polyethylene ECC would not significantly change as a result of an increase in the ultimate tensile strain of the material. On the other hand, the MOR of the 2% polyethylene ECC can be increased by increasing the tensile first-cracking strength and/or the ultimate tensile strength.

The results of this model can be used in conjunction with micromechanical models of tensile properties of ECC materials to optimize their flexural

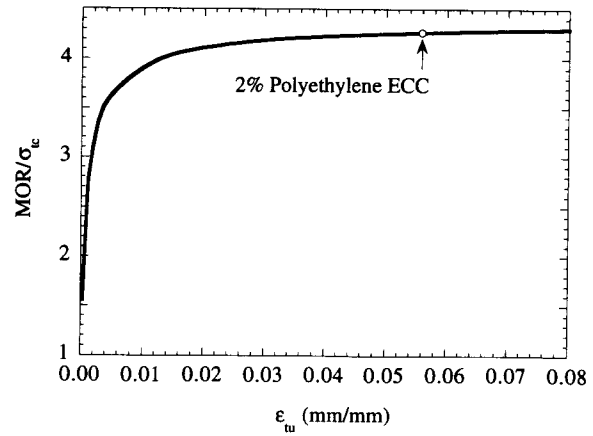

FIG. 13. Variation of MOR-to-σ_{tc} Ratio as Function of Ultimate Tensile Strain

strength. Li (1993) showed that the tensile first-cracking strength, the ultimate tensile strength, and the ultimate tensile strain can be increased while maintaining a low-fiber-volume fraction by proper tailoring of the micromechanical parameters (fiber, matrix, and fiber/matrix interface properties) according to micromechanical models constructed on the basis of fracture mechanics and deformation mechanisms.

CONCLUSIONS

In this paper it was found that the strain-hardening behavior gives ECC materials a significant advantage under flexural loading. In a third-point bending test, the flexural strength of an ECC was measured to be five times its tensile (first-cracking) strength. In contrast, for quasi-brittle materials, such as the 1% steel-fiber composite, the ratio of flexural strength to tensile strength has an upper bound of 3. The positive effect of strain hardening on the flexural/tensile-strength ratio was also predicted by a simple theoretical model. The model suggests that the flexural strength of ECC materials can be increased by increasing the strain capacity, the tensile first-cracking strength, and/or the ultimate tensile strength of the material.

ACKNOWLEDGMENTS

Part of this work has been supported by a grant MSS-9301949 from the National Science Foundation to the University of Michigan. A gift from the U.S. Gypsum Corp., Libertyville, Ill., to the Advanced Civil Engineering Materials Research Laboratory, at the university is also gratefully acknowledged. A U-M. Rackham Predoctoral Fellowship Award supported the doctoral study of M. Maalej.

APPENDIX I. EQUATIONS FOR M AND ε_t (BILINEAR STRESS DISTRIBUTION)

$$\varepsilon_t = \frac{-a_1(\mathbf{v}) - [a_1(\mathbf{v})^2 - 4a_0(\mathbf{v})a_2(\mathbf{v})]^{1/2}}{2a_0(\mathbf{v})} \tag{11}$$

where

$$\mathbf{v} = (\sigma_{tc}, \varepsilon_{tc}, \sigma_{tu}, \varepsilon_{tu}, \sigma_{cp}, \varepsilon_{cp}, r) \tag{12}$$

$$a_0(\mathbf{v}) = -6\sigma_{cp}(\varepsilon_{tu} - \varepsilon_{tc})(1 - r)^2 + 12\varepsilon_{cp}(\sigma_{tu} - \sigma_{tc})r^2 \tag{13}$$

$$a_1(\mathbf{v}) = 12\sigma_{cp}(\varepsilon_{tu} - \varepsilon_{tc})(\varepsilon_{tc} - \varepsilon_{cp}r)(1 - r) + 24\varepsilon_{cp}(\varepsilon_{tu}\sigma_{tc} - \varepsilon_{tc}\sigma_{tu})r^2 \tag{14}$$

$$a_2(\mathbf{v}) = 2\sigma_{cp}(\varepsilon_{tu} - \varepsilon_{tc})(\varepsilon_{cp}^2 r^2 + 6\varepsilon_{cp}\varepsilon_{tc}r - 3\varepsilon_{tc}^2) - 12\varepsilon_{tc}\varepsilon_{cp}(\varepsilon_{tu}\sigma_{tc} - \varepsilon_{tc}\sigma_{tu})r^2 \tag{15}$$

and

$$M = \left(\frac{bd^2}{6}\right)\frac{b_0(\mathbf{v}) + b_1(\mathbf{v})\varepsilon_t + b_2(\mathbf{v})\varepsilon_t^2 + b_3(\mathbf{v})\varepsilon_t^3}{108\varepsilon_{cp}(\varepsilon_t - \varepsilon_{tc})^2(\varepsilon_{tc} - \varepsilon_{tu})} \tag{16}$$

where

$$b_0(\mathbf{v}) = 6\sigma_{cp}(\varepsilon_{tu} - \varepsilon_{tc})(18\varepsilon_{tc}^3 - 27\varepsilon_{cp}\varepsilon_{tc}^2 r + \varepsilon_{cp}^3 r^3)$$

$$+ 108\varepsilon_{cp}\varepsilon_{tc}^2(\varepsilon_{tu}\sigma_{tc} - \varepsilon_{tc}\sigma_{tu})r^3 \quad (17)$$

$$b_1(\mathbf{v}) = 54\sigma_{cp}(\varepsilon_{tu} - \varepsilon_{tc})[-6\varepsilon_{tc}^2 + 3\varepsilon_{tc}(2\varepsilon_{cp} + \varepsilon_{tc})r + \varepsilon_{cp}^2 r^3] - 324\varepsilon_{cp}\varepsilon_{tc}(\varepsilon_{tu}\sigma_{tc} - \varepsilon_{tc}\sigma_{tu})r^3 \quad (18)$$

$$b_2(\mathbf{v}) = 162\sigma_{cp}(\varepsilon_{tu} - \varepsilon_{tc})(2\varepsilon_{tc} - 2\varepsilon_{tc}r - \varepsilon_{cp}r + \varepsilon_{cp}r^3) + 324\varepsilon_{cp}(\varepsilon_{tu}\sigma_{tc} - \varepsilon_{tc}\sigma_{tu})r^3 \quad (19)$$

$$b_3(\mathbf{v}) = 54\sigma_{cp}(\varepsilon_{tu} - \varepsilon_{tc})(-2 + 3r - r^3) + 108\varepsilon_{cp}(\sigma_{tu} - \sigma_{tc})r^3 \quad (20)$$

APPENDIX II. EQUATIONS FOR M AND ε_t (LINEAR STRESS DISTRIBUTION)

$$\varepsilon_t = \frac{-a_1(\mathbf{v}) - [a_1(\mathbf{v})^2 - 4a_0(\mathbf{v})a_2(\mathbf{v})]^{1/2}}{2a_0(\mathbf{v})} \quad (21)$$

where

$$\mathbf{v} = (\sigma_{tc}, \varepsilon_{tc}, \sigma_{tu}, \varepsilon_{tu}, \sigma_{cp}, \varepsilon_{cp}, r) \quad (22)$$

$$a_0(\mathbf{v}) = -2\sigma_{cp}(\varepsilon_{tu} - \varepsilon_{tc})(1 - r)^2 + \varepsilon_{cp}(\sigma_{tu} - \sigma_{tc})r^2 \quad (23)$$

$$a_1(\mathbf{v}) = 4\sigma_{cp}\varepsilon_{tc}(\varepsilon_{tu} - \varepsilon_{tc})(1 - r) + 2\varepsilon_{cp}(\varepsilon_{tu}\sigma_{tc} - \varepsilon_{tc}\sigma_{tu})r^2 \quad (24)$$

$$a_2(\mathbf{v}) = \varepsilon_{tc}[-2\sigma_{cp}\varepsilon_{tc}(\varepsilon_{tu} - \varepsilon_{tc}) - \varepsilon_{cp}(\varepsilon_{tu}\sigma_{tc} - \varepsilon_{tc}\sigma_{tu})r^2] \quad (25)$$

and

$$M = \left(\frac{bd^2}{6}\right)\frac{b_0(\mathbf{v}) + b_1(\mathbf{v})\varepsilon_t + b_2(\mathbf{v})\varepsilon_t^2 + b_3(\mathbf{v})\varepsilon_t^3}{108\varepsilon_{cp}(\varepsilon_t - \varepsilon_{tc})^2(\varepsilon_{tc} - \varepsilon_{tu})} \quad (26)$$

where

$$b_0(\mathbf{v}) = 108\varepsilon_{tc}^2[4\sigma_{cp}\varepsilon_{tc}(\varepsilon_{tu} - \varepsilon_{tc}) + \varepsilon_{cp}(\varepsilon_{tu}\sigma_{tc} - \varepsilon_{tc}\sigma_{tu})r^3] \quad (27)$$

$$b_1(\mathbf{v}) = 324\varepsilon_{tc}[2\sigma_{cp}\varepsilon_{tc}(\varepsilon_{tu} - \varepsilon_{tc})(r - 2) - \varepsilon_{cp}(\varepsilon_{tu}\sigma_{tc} - \varepsilon_{tc}\sigma_{tu})r^3] \quad (28)$$

$$b_2(\mathbf{v}) = 324[4\sigma_{cp}\varepsilon_{tc}(\varepsilon_{tu} - \varepsilon_{tc})(1 - r) + \varepsilon_{cp}(\varepsilon_{tu}\sigma_{tc} - \varepsilon_{tc}\sigma_{tu})r^3] \quad (29)$$

$$b_3(\mathbf{v}) = 108[-2\sigma_{cp}(\varepsilon_{tu} - \varepsilon_{tc})(2 - 3r + r^3) + \varepsilon_{cp}(\sigma_{tu} - \sigma_{tc})r^3] \quad (30)$$

APPENDIX III. REFERENCES

Aveston, J., Mercer, R. A., and Sillwood, J. M. (1974). "Fiber reinforced cements—Scientific foundations for specifications." *Composites standards testing and design*, IPC Science and Technology Press, Guildford, U.K., 93–103.

Hillerborg, A., Modéer, M., and Petersson, P. E. (1976). "Analysis of crack formation and crack growth in concrete by means of fracture mechanics and finite elements." *Cement and Concr. Res.*, 6(6), 773–782.

Krenchel, H., and Stang, H. (1988). "Stable microcracking in cementitious materials." *Proc. 2nd Int. Symp. on Brittle Matrix Composites—BMC 2*, A. M. Brandt and I. H. Marshall, eds., Elsevier Applied Science, London, England, 20.

Li, V. C. (1993). "From micromechanics to structural engineering—The design of cementitious composites for civil engineering applications." *J. Struct. Mech. and Earthquake Engrg.*, Tokyo, Japan, 10(2), 37–48.

Li, V. C., and Hashida, T. (1992). "Ductile fracture in cementitious materials?" *Fracture mechanics of concrete structures*, Z. P. Bazant, ed., Elsevier Applied Science, London, England, 526–535.

Li, V. C., and Leung, C. K. Y. (1992). "Steady state and multiple cracking of short random fiber composites." *J. Engrg. Mech.*, ASCE, 118, 2246–2264.

Li, V. C., Maalej, M., and Hashida, T. (1994). "Experimental determination of stress-crack opening relation in fiber cementitious composites with crack tip singularity." *J. Mater. Sci.*, 29(10), 2719–2724.

Maalej, M. (1994). "Fracture resistance of engineered fiber cementitious composites and implications to structural behavior," PhD thesis, University of Michigan, at Ann Arbor, Mich.

Maalej, M., and Li, V. C. (1994). "Flexural strength of fiber cementitious composites." *J. Mater. in Civ. Engrg.*, ASCE, 6(3), 390–406.

Marshall, D., and Cox, B. N. (1988). "A J-integral method for calculating steady-state matrix cracking stress in composites." *Mech. of Mater.*, 7(2), 127–133.

Mishra, D. K. (1994). "Performance of engineered cementitious composites under shear load," PhD thesis, University of Michigan, at Ann Arbor, Mich.

Ward, R., and Li, V. C. (1990). "Dependence of flexural behavior of fiber reinforced mortar on material fracture resistance and beam size." *ACI J. Mater.*, 87(6), 627–637.

Zhu, Y. (1990). "The flexural strength function for concrete beams without initial cracks." *Proc. 8th European Congress of Fracture: Fracture Behavior and Design of Mater. and Struct.*, Vol. 2, D. Firrao, ed., Chameleon Press Ltd., London, England, 599–604.

"Standard test method for flexural strength of concrete (using simple beam with third-point loading)." (1983). *ASTM C78-75, 1983 annual book of ASTM Standards*, Vol. 04.02, ASTM, Philadelphia, Pa., 39–41.

APPENDIX IV. NOTATION

The following symbols are used in this paper:

- a = depth of inelastic microcracking zone;
- b = specimen width;
- c = distance from extreme tension fiber to neutral axis;
- d = specimen depth;
- e = distance from extreme tension fiber to point where material changes stiffness in compression;
- L = span length;
- M = externally applied bending moment;
- M_u = ultimate moment capacity;
- r = depth of inelastic microcracking zone normalized by specimen depth;
- r_c = r value when compressive strain at extreme compression fiber equals material's compressive strain at peak stress;
- r_t = r value when tensile strain at extreme tension fiber equals material's ultimate tensile strain;
- r_u = smallest of r_c and r_t;
- x = distance from extreme tension fiber to arbitrary point along depth of beam;
- $\varepsilon(x)$ = strain at point x;
- ε_c = compressive strain at extreme compression fiber;
- ε_{cp} = compressive strain at peak stress;
- ε_t = tensile strain at extreme tension fiber;
- ε_{tc} = tensile first-cracking strain;
- ε_{tu} = ultimate tensile strain;
- ρ = beam radius of curvature;

$\sigma(x)$ = stress at point x;
σ_{cp} = compressive strength;
σ_f = flexural stress corresponding to M;
σ_{tc} = tensile first-cracking strength; and
σ_{tu} = ultimate tensile strength.

Flexural/Tensile-Strength Ratio in Engineered Cementitious Composites

By Mohamed Maalej[1] and Victor C. Li,[2] Members, ASCE

Abstract: In this paper the flexural behavior of a strain-hardening engineered cementitious composite (ECC) is studied and compared with that observed in a regular fiber-reinforced cementitious composite (FRC). Unlike concrete or regular FRC, ECC materials are characterized by their ability to sustain higher levels of loading after first cracking while undergoing additional straining. This strain-hardening behavior gives ECCs a significant advantage under flexural loading. In quasi-brittle material such as regular FRC, the ratio of flexural strength (the modulus of rupture) to tensile strength is known to vary between 1 and 3, depending on the details of the reinforcement and the geometry of the specimen. In this paper, the strain-hardening behavior observed in an ECC led to a high flexural-strength–to–tensile-strength ratio. In a third-point bending test, the flexural strength of an ECC was measured to be five times its tensile (first-cracking) strength. This result was also predicted by a simple theoretical model. The model can be used for the purpose of optimizing the flexural strength of ECCs.

INTRODUCTION

Three types of tensile failure modes have been observed in cementitious materials (see Fig. 1 for a schematic illustration): brittle, quasi-brittle, and ductile failure. Brittle failure can be observed in hardened cement paste material. It is characterized by a linear stress-strain curve (curve A) followed by a sudden drop in stress at first cracking with an ultimate tensile strain in the order of 0.01%. Quasi-brittle failure can be observed in concrete and most fiber-reinforced cements and concretes. It is characterized by a linear stress-strain curve (curve B) followed by a softening tail (tension-softening curve), after first cracking, due to the bridging action of aggregates, cement ligaments, and/or fibers. The ultimate tensile strain of quasi-brittle materials is of the same order of magnitude as that for brittle materials, although the material toughness is enhanced by inelastic energy absorption in the post-peak regime. For both brittle and quasi-brittle materials, the first cracking strength corresponds to the tensile strength of the material. Ductile failure can be observed in continuous aligned fiber-reinforced cement materials (Aveston et al. 1974; Krenchel and Stang 1988). Ductile materials are characterized by their ability to sustain higher levels of loading after first cracking while undergoing large deformation (curve C). Recently ductile failure has also been observed in short-fiber cementitious composites of low-fiber-volume fractions (Li 1993; Li and Hashida 1992) (e.g., 2% for polyethylene-fiber composites). These composites have been designed according to micromechanical models that are constructed on the basis of micromechanics of defect growth in a brittle matrix composite whereby crack bridging is provided by fibers to achieve steady state cracking (Li and Leung 1992;

[1]Res. Fellow, Advanced Civ. Engrg. Mater. Res. Lab., Dept. of Civ. and Envir. Engrg., Univ. of Michigan, 2326 G.G. Brown Bldg., Ann Arbor, MI 48109-2125.
[2]Prof., Advanced Civ. Engrg. Mater. Res. Lab., Dept. of Civ. and Envir. Engrg., Univ. of Michigan, Ann Arbor, MI.

Note. Discussion open until April 1, 1995. To extend the closing date one month, a written request must be filed with the ASCE Manager of Journals. The manuscript for this paper was submitted for review and possible publication on January 24, 1994. This paper is part of the ***Journal of Materials in Civil Engineering***, Vol. 6, No. 4, November, 1994. ©ASCE, ISSN 0899-1561/94/0004-0513/$2.00 + $.25 per page. Paper No. 7737.